Polymer Vol. 37 No. 12, pp. 2423–2431, 1996

0032-3861/96/$15.00+0.00

Studies on the miscibility of blends of polychloroprene and poly(ethylene–methyl acrylate) copolymer

P. P. Kundu and D. K. Tripathy*
Rubber Technology Centre, Indian Institute of Technology, Kharagpur 721302, India

and S. Banerjee
Defence Research and Development Establishment (DRDO), Jhansi Road, Gwalior 474002, India
(Received 27 June 1995; revised 22 November 1995)

Studies on blends of polychloroprene (CR) and poly(ethylene–methyl acrylate) copolymer (PEMA) have been carried out with respect to their miscibility. Irrespective of the methods of measurement used, such as differential scanning calorimetry (d.s.c.) or dynamic mechanical analysis (d.m.a.), these blends show a single glass transition temperature and also obey the Fox law. The crystallinity, measured by wide-angle X-ray diffraction (WADX), as well as the crystalline melting temperature (from d.s.c. and d.m.a.), decreases with the increasing CR content of the blends. The lowering of the crystalline melting temperature of PEMA leads to a negative interaction parameter between PEMA and CR. The miscibility of the PEMA/CR blends has also been investigated by using Fourier transform infra-red (*FT* i.r.) spectroscopy. A lowering of the CH_3 asymmetric stretching frequency of PEMA with an increasing amount of CR in the PEMA/CR blends indicates a dipolar interaction between the polar methyl acrylate and chloride groups. Examination of the cryogenically fractured surfaces using scanning electron microscopy (SEM) shows that the blends of PEMA and CR are well dispersed. These studies confirm the miscibility of PEMA and CR for all of the blend compositions. Copyright © 1996 Elsevier Science Ltd.

(Keywords: miscibility; blend composition; CR/PEMA blends)

INTRODUCTION

Blending is a technique for generating a new polymer system with improved properties compared to its individual constituents. From the thermodynamic point of view, a blend is 'miscible' only when the Gibbs free energy of mixing (ΔG_m) is negative, i.e. when $\Delta G_m < 0$. The expression for the Gibbs free energy is given by:

$$\Delta G_m = \Delta H_m - T\Delta S_m \quad (1)$$

A unique feature which affects the thermodynamics of polymer blends when compared to other systems are the large values of the molecular weights of both components. The entropy of mixing (ΔS_m) in equation (1) will be very small owing to the comparatively small number of molecules of each polymer in the blend. Therefore, a blend is thermodynamically favourable only when the enthalpy of mixing (ΔH_m) is negative. The latter can have both dispersive and specific components. Two non-polar polymers with matching solubility parameters can be blended together to obtain a miscible system due to the weak dispersive or van der Waals interaction. When the components are sufficiently polar, the weak dispersive and strong specific interactions give positive and negative contributions, respectively, towards ΔH_m, as follows[1]:

$$\Delta H_m = +\Delta H_m(\text{dis}) - N\Delta H_m(\text{sp}) \quad (2)$$

where N is the number of specific interactions. In the presence of a sufficient number of specific interactions, the polymer blends are found to be thermodynamically miscible.

Miscibility can be measured by various methods[2–9]. The easiest way to measure miscibility is through the measurement of the glass transition temperatures (T_gs) of the blends and their constituent polymers. These parameters can be measured either by d.m.a.[10–14] or by d.s.c.[15–17]. According to the Fox equation[18], the following relationship is found:

$$\frac{1}{T_{g(b)}} = \frac{W_1}{T_{g(1)}} + \frac{W_2}{T_{g(2)}} \quad (3)$$

where $T_{g(b)}$ is the glass transition temperature of the blend, and $T_{g(1)}$ and $T_{g(2)}$ are the glass transition temperatures of the constituent polymers (1) and (2), with respective weight fractions of W_1 and W_2.

Apart from the composition-dependent single T_g, the lowering of the melting temperature of a crystalline polymer on blending with an amorphous polymer can also be used in determination of the miscibility. Nishi

* To whom correspondence should be addressed

and Wang[19] have shown that the following relationship applies in this case:

$$\frac{1}{T_m} - \frac{1}{T_m^o} = -\frac{R\bar{V}_2}{\Delta H_2 \bar{V}_1} X'_{12}\phi_1^2 \quad (4)$$

where T_m^o and T_m are, respectively, the equilibrium melting temperatures of the crystalline polymer and its blend with the amorphous polymer, ΔH_2 is the heat of fusion per repeating chain segment of the crystalline polymer, $\bar{V}_1$ and $\bar{V}_2$ are, respectively, the molar volumes of the repeating chain segments of the crystalline and amorphous polymers, X'_{12} is the interaction parameter between the polymers in the blend, and ϕ_1 is the volume fraction of amorphous polymer in the blend. If $T_m^o > T_m$, i.e. there is a lowering of the crystalline melting temperature, then X'_{12} obtained from equation (4) will be negative, which gives direct evidence of the miscibility of the component polymers[19].

Miscibility can also be studied by Fourier transform infra-red (*FT*i.r.) spectroscopy. The characteristics i.r. group frequencies[20,21] of a polymer may either remain unchanged or shift in a definite direction on blending with another polymer, leading to either a non-interactive or an interactive polymer blend. For a miscible polymer blend, *FT*i.r. spectroscopy can be used as a tool for qualitative measurement of the miscibility[22,23].

EXPERIMENTAL

Materials

The details of the materials used in this study are given in *Table 1*.

Sample preparation

The polymers were mixed in a Brabender Plasticorder (PLE-330) machine provided with a cam-type rotor, according to the formulations given in *Table 2*. Thermoplastic PEMA was first melted in the chamber at 100°C for 2 min at a rotor speed of 40 r.p.m., followed by addition of the premasticated CR (neoprene). To ensure proper mixing, the blending was carried out at 100 r.p.m., at a temperature of 100°C for 5 min. The hot blend was then removed from the chamber and quickly passed through a two-roll mill with a low nip gap to form a sheet. Moulding of the sheet was carried out in an hydraulic press (Moore Press) at 100°C, at a pressure of 1 MPa.

Dynamic mechanical analysis (d.m.a.)

Dynamic mechanical analysis of the samples was carried out by using a Dynamic Rheovibron Viscoelastometer (Model DDV-III-EP, Orientec Corporation, Japan). Samples with dimensions of $70 \times 10 \times 5\,mm^3$ were cut from the moulded sheets. The storage modulus and $\tan\delta$ values were measured at a frequency of 11 Hz in the temperature range from -150 to 100°C under a programmed heating rate of $2°C\,min^{-1}$ from the lowest to the highest temperature. Results were scanned isochronally over a wide range of temperatures.

Differential scanning calorimetry (d.s.c.)

Differential scanning calorimetry studies were carried out on a thermal analyser (Du Pont-9000) in the temperature range from -150 to 100°C at a heating rate of $20°C\,min^{-1}$. All results were recorded for the first heating run of the samples.

Wide-angle X-ray diffraction (WAXD)

An X-ray diffractometer with a scintillation counter (Rigaku Corporation, Japan) was used to obtain scanning intensity curves for values of 2θ ranging from 10 to 30°. Samples with dimensions of $60 \times 30 \times 5\,mm^3$ were cut from the sheets and used for X-ray analysis. The incident X-ray beam (CuKα, 40 kV, 25 mA) was passed through a Ni filter, and a pulse-height discriminator was used to achieve further monochromatization. All of the X-ray diffraction patterns that were obtained showed crystalline peaks which were superimposed on an amorphous halo. The degree of crystallinity (X_c) was recorded from the ratio of the areas under the crystalline peaks and the respective amorphous halos by using the method of Hermans and Weidinger[24]. The size of the crystalline regions (P) was determined from the broadening of the peaks by using the Scherrer formula[25], as follows:

$$P = \frac{0.89\lambda}{\beta\cos\theta} \quad (5)$$

where β is the half-width, θ is the Bragg angle and λ is the wavelength. The interchain separation (R) in the amorphous region of the samples was evaluated from the position of the maximum of the halo by using the relationship given by Klug and Alexander[26], as follows:

$$R = \frac{5\lambda}{8\sin\theta} \quad (6)$$

Table 1 Details of the polymers used in this study

Polymer	Details[a]	Supplier
Poly(ethylene–methyl acrylate)	Trade name: OPTEMATC-120 Melt index: $6.0\,dg\,min^{-1}$ Density: $940\,kg\,m^{-3}$ Methyl acrylate content: 21 wt % Melting point: 81°C M_w: 220 700	Exxon Chemicals, USA
Polychloroprene	Trade name: Neoprene WM1 Specific gravity: 1.23 Mooney viscosity: 40 (ML_{1+4}, 120°C)	Du Pont, USA

[a] As provided by the supplier

Table 2 Blend compositions (wt %) used in this study

Component	A	B	C	D	E
PEMA	100	70	50	30	0
CR	0	30	50	70	100

FTi.r.-attenuated total reflectance (ATR) spectroscopy

A Perkin-Elmer 1720X FT-IR spectrometer equipped with a DTGS detector and a flat-plate ATR sampling accessory was used to obtain the i.r. spectra. A thallium/iodide (KRS-5) parallelogram crystal with an angle of incident of 45° was employed. All of the ATR spectra were collected at 4 cm^{-1} resolution, with 50 scans being accumulated for each sample. Three sets of spectra were recorded for each sample and were found to be identical.

Scanning electron microscopy (SEM)

Cryogenically fractured samples were used for the scanning electron microscopy studies. The samples were coated with gold for a period of 1 min by using a sputter machine and then vacuum dried for 20 min. Micrographs were obtained by using a Cam Scan Series 2 scanning electron microscope.

RESULTS AND DISCUSSIONS

D.m.a. studies

The variation of the loss tangent with temperature for the various blends is plotted in *Figure 1*, with the peak values given in *Table 3*.

Pure PEMA, which is amorphous, shows four transitions; these features are strikingly similar to those observed for the transition behaviour of completely amorphous linear polyethylene produced by rapid quenching of very thin specimens[27,28].

The γ-relaxation at −131.2°C is associated with the freezing-in of the movement of the polar methyl acrylate groups in the amorphous phase, coupled with defects or dislocations in the lamelar crystal structure[28].

The β_u-relaxation at −77.0°C is associated with the glass–rubber relaxation of unconstrained amorphous poly(ethylene–methyl acrylate)[27], while the β_c-relaxation at −18.0°C corresponds to the crystal-constrained glass–rubber relaxation[29]. This is the reason for the broadness of the β-relaxation. As the β-relaxation is associated with the catastrophic fall in the storage modulus (see *Figure 2*), it represents the main glass–rubber relaxation due to the freezing-in of long-range, main-chain segmental motions.

The peak at −105°C corresponds to the γ-transition which is associated with small-scale segmental motions

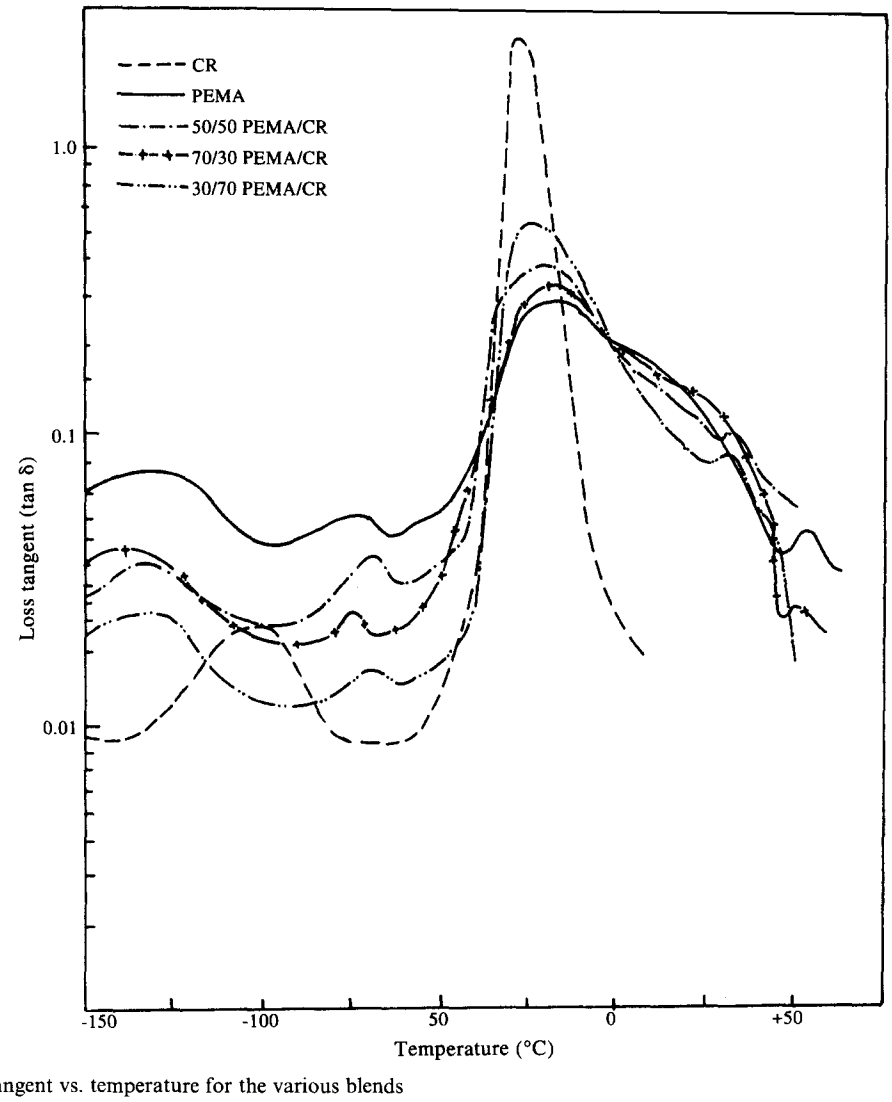

Figure 1 Plots of loss tangent vs. temperature for the various blends

Table 3 Results obtained from dynamic mechanical analysis of the various blends

Blend	α-Relaxation temperature (°C)	β-Relaxation temperature (°C)		β-Relaxation zone, ΔT (°C)	$\tan\delta_{max}$	γ-Relaxation temperature (°C)
		Unconstrained	Constrained, T_{max}			
A	51.5	−77.0	−18.0	53.0	0.269	−131.2
B	48.5	−75.0	−20.0	42.0	0.296	−131.0
C	30.0	−73.0	−21.3	38.0	0.354	−131.0
D	27.5	−71.3	−23.2	35.0	0.502	−129.0
E	–	–	−26.0	14.0	2.000	−105.0

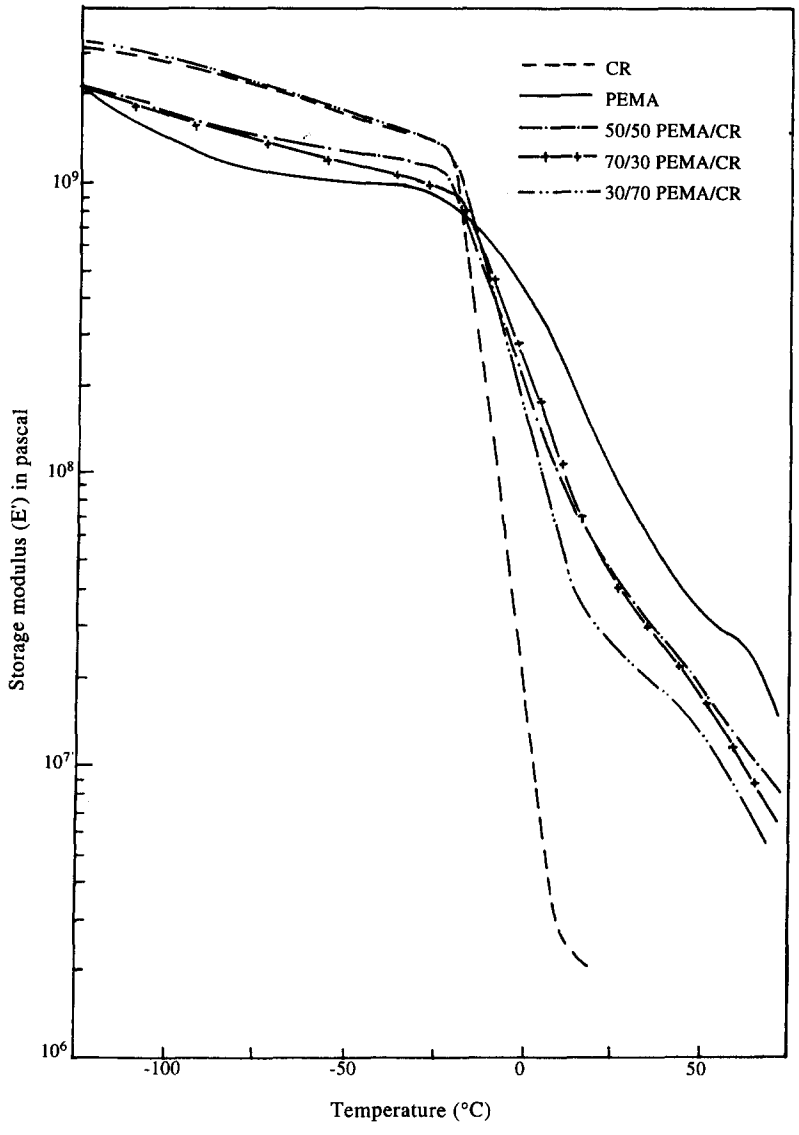

Figure 2 Plots of storage modulus vs. temperature for the various blends

in the amorphous polychloroprene. The peak at −26.0°C corresponds to the β-transition where the storage modulus falls catastrophically (see *Figure 2*). It is believed that the β-process represents the glass–rubber transition which is associated with long-range segmental motions.

The peaks observed at −131.0, −131.0, and −129.0°C, correspond to the γ-transition temperatures for the 70/30, 50/50 and 30/70 PEMA/CR blends, respectively. The relaxations at −75.0, −73.0, and −71.3°C are associated, respectively, with the unconstrained glass–rubber transitions of the 70/30, 50/50, and 30/70 PEMA/CR blends.

The peaks at −20.0, −21.3, and −23.2°C, corresponding to the maximum loss tangent peak temperatures (T_{max}s), are associated, respectively, with the glass transition temperatures of the 70/30, 50/50 and 30/70 PEMA/CR blends. These results are in good agreement with the corresponding theoretical values of −19.8, −21.3, and −22.9°C, obtained from the Fox equation.

The peak at +51.5°C is associated with the crystalline

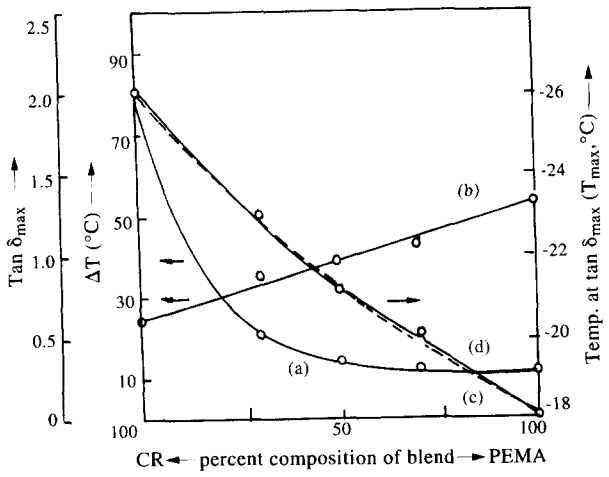

Figure 3 The effect of blend composition on: (a) $\tan\delta_{max}$; (b) the β-relaxation zone, ΔT; (c) theoretical T_{max}; (d) experimental T_{max}

Table 4 Results obtained from differential scanning calorimetry studies of the various blends

Blend	T_g (°C)	T_m (°C)	Volume fraction of CR, ϕ_1	Negative interaction parameter, $-X'_{12}$[a]
A	−53.5	45.2	–	–
B	−46.5	41.7	0.24	0.122
C	−42.6	40.5	0.42	0.053
D	−42.0	39.3	0.63	0.030
E	−39.0	37.5	–	–

[a] Calculated from equation (4) by using $\Delta H_2 = 1533.4\,J\,mol^{-1}$ for the repeating segment of PEMA, $\bar{V}_1 = 69.14\,cm^3\,mol^{-1}$ for the repeating segment of CR, and $\bar{V}_2 = 63.7\,cm^3\,mol^{-1}$ for the repeating segment of PEMA

melting temperature of PEMA, while the transitions at 48.5, 30.0, and 27.5°C are associated, respectively, with the crystalline melting temperatures of the 70/30, 50/50 and 30/70 PEMA/CR blends.

A plot of the maximum peak value of tan δ against percent composition of the blends shows a concave curve which falls below the tie line (*Figure 3a*). This curve indicates that the high $\tan\delta_{max}$ value of CR drops sharply up to a value of 30% blending with PEMA; above this level any further changes in the $\tan\delta_{max}$ values of the blends are negligible.

The glass transition temperatures of the individual polymers and their blends when plotted against composition (%) show a concave curve[30] which falls below the tie line (*Figure 3d*). The theoretical values of the T_gs obtained from the Fox equation also show a similar trend (*Figure 3c*).

Figure 2 shows the variation of the storage modulus of the blends with temperature. Polychloroprene (CR) shows a sharp drop in modulus, whereas in the case of PEMA the drop is gradual in the β-relaxation zone. For all of the blends the temperature corresponding to the drop in the storage modulus lies between the values of the individual polymers. The temperature difference (ΔT) is a measure of the broadness of the β-relaxation. *Figure 3b* shows that the broadness of the β-relaxation of PEMA reduces with the increased CR content in the blends.

D.s.c. studies

Plots of heat flow against temperature for the individual polymers and the various blends are shown in *Figure 4*, with the corresponding peak values given in *Table 4*.

Polychloroprene shows a sharp baseline shift at −39.0°C, which is associated with the glass–rubber transition; the sharpness is due to the sudden drop of

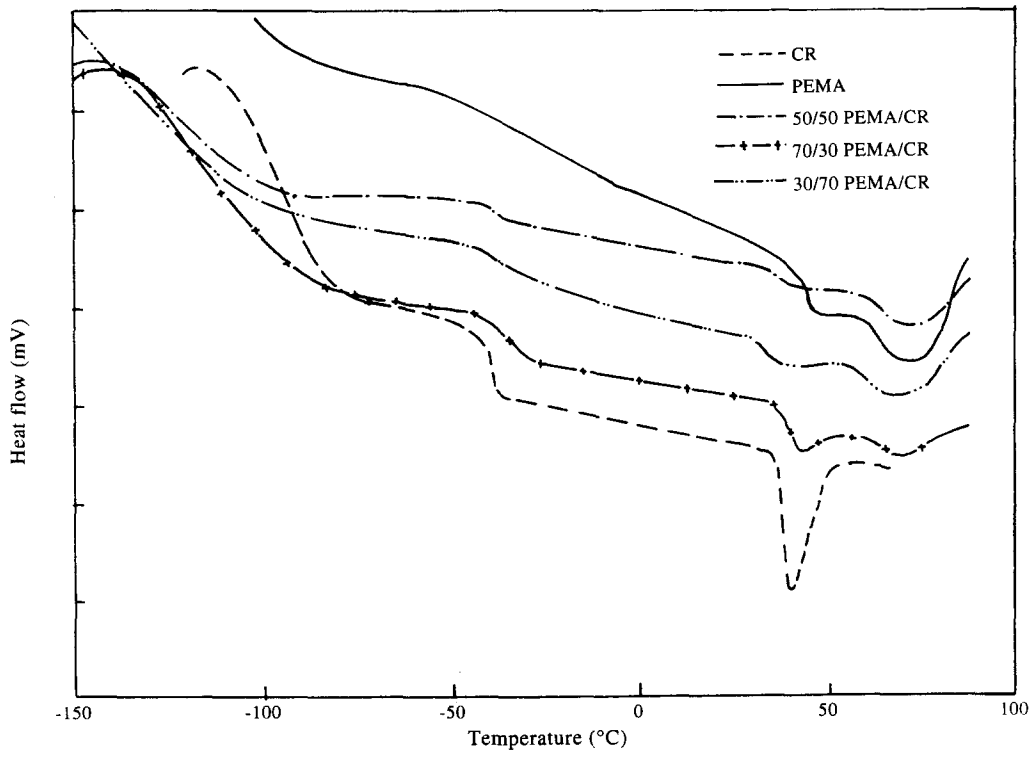

Figure 4 Plots of heat flow vs. temperature for the various blends

heat capacity of the amorphous CR at this temperature. The transition at −53.5°C is associated with the glass–rubber transition of low crystallinity PEMA. This peak is broad, as this is a crystal-hindered transition. The transitions at −46.5, −42.6, and −42.0°C are associated, respectively, with the glass–rubber transition temperatures of the 70/30, 50/50, and 30/70 PEMA/CR blends. These values are in good agreement with the corresponding theoretical values of −48.1, −45.1, and −42.0°C obtained from the Fox equation.

The glass transition temperatures of the individual polymers and their blends are plotted against blend composition in *Figure 5a*. The plot is concave and shows a positive deviation in comparison to the theoretical values given by the Fox law. The theoretical T_g values of the blends also follow a concave variation. The sharp transition at 37.5°C is associated with the crystalline melting temperature of amorphous CR, where the sharpness of the peak is probably due to the presence of a small number of large crystallites in the CR. The crystalline melting temperature of PEMA at 45.2°C is broad with melting being completed at 75.0°C. The broadness of this peak is probably due to the presence of a comparatively large number of smaller crystallites in the PEMA. The transitions at 41.7, 40.5, and 39.3°C are associated, respectively, with the crystalline melting temperatures of the 70/30, 50/50 and 30/70 PEMA/CR blends.

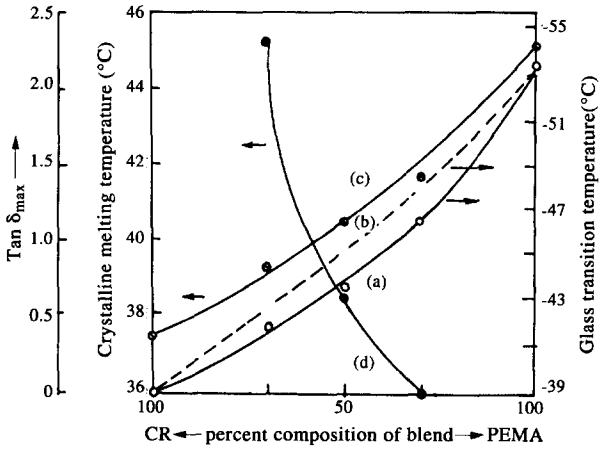

Figure 5 The effect of blend composition on: (a) experimental T_g; (b) theoretical T_g; (c) T_m; (d) $-X'_{12}$

The crystalline melting temperature of the individual polymers and their blends are plotted against the blend composition in *Figure 5c*. The plot is concave and shows a negative deviation with respect to the additive values of the components. On increasing the amorphous CR content in the blends, the crystalline melting temperature of PEMA is reduced[31]. The interaction parameters between PEMA and CR, calculated from equation (4), are all negative[32], as shown in *Table 4*. The plot of negative interaction parameter ($-X'_{12}$) *versus* blend composition (*Figure 5d*) shows that $-X'_{12}$ decreases sharply up to a level of 40% blending with CR, beyond which it then gradually decreases.

WAXD studies

Plots of the X-ray diffraction intensities as a function of 2θ for the individual polymers and their various blends are shown in *Figure 6*. The amorphous halos appear in the regions from 16.2 to 22.1°, 18.6 to 22.1°, 18.6 to 21.3°, 18.2 to 21.5°, and 18.8 to 19.2°, with corresponding peak values at 20.8, 20.7, 19.1, 19.05, and 19.0° for PEMA, the 70/30, 50/50, and 30/70 PEMA/CR blends, and CR, respectively. Addition of CR to the blend increases the broadness and decreases the intensity of the PEMA peak (*Figure 6*). The values representing the strongest peaks are shown in *Table 5*.

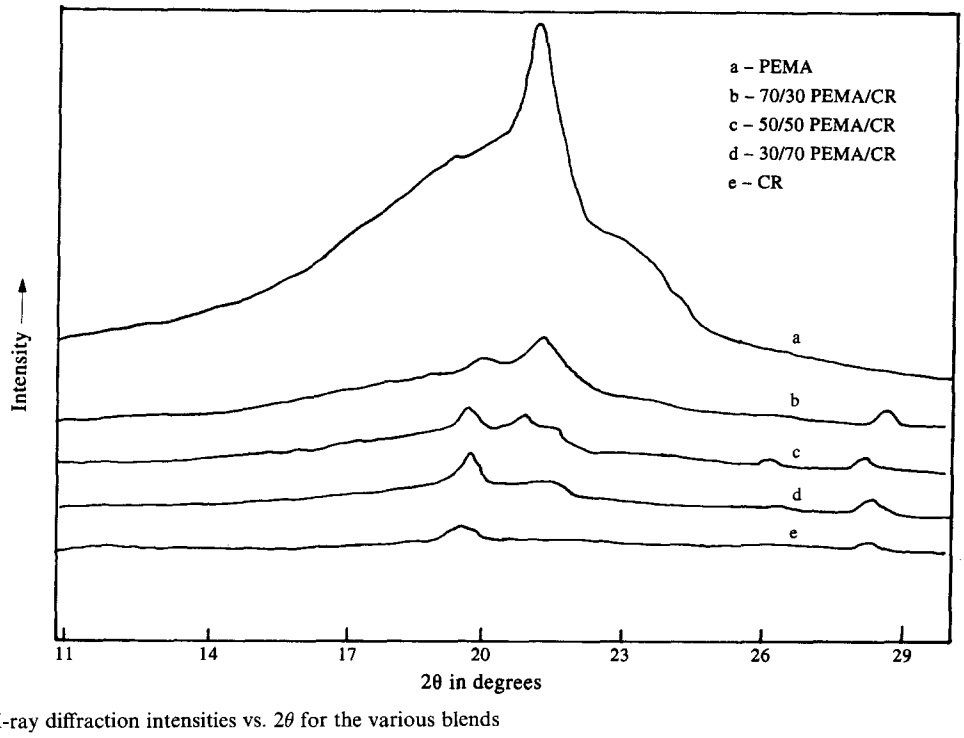

Figure 6 Plots of X-ray diffraction intensities vs. 2θ for the various blends

Table 5 Results obtained from wide-angle X-ray diffraction studies of the various blends

Blend	Extent of crystallinity, X_c (%)	Interchain separation, R (nm)	Crystallite size, P (nm)
A	14.0	0.275	6.1
B	11.8	0.273	10.5
C	8.5	0.294	16.1
D	7.4	0.295	18.1
E	4.4	0.294	18.1

Table 6 Major *FT* i.r. absorption peaks (cm^{-1}) present in the various blends

Assignment	PEMA	PEMA/CR blends 70/30	50/50	30/70
CH_3 asymmetric stretch	1465	1455	1448	1440
>C=O stretch	1736	1736	1736	1736
C–O–C symmetric stretch	1227	1227	1227	1227
C=C stretch	–	1658	1658	1658
C–Cl overtone	–	1451	1451	1451

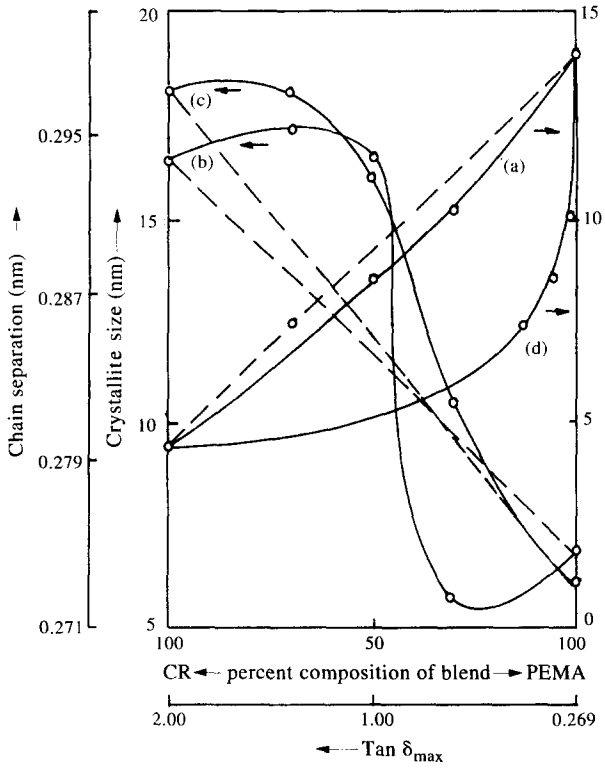

Figure 7 The effect of blend composition on: (a) the extent of crystallinity; (b) interchain separation; (c) crystallite size. The extent of crystallinity as a function of tan δ_{max} is shown in (d)

Figure 7a shows the decrease in the extent of crystallinity with the increasing CR content of the various blends. The concave nature of the plot indicates a negative deviation from the additive values. The corresponding plot for the interchain separation as a function of blend composition (*Figure 7b*) is concave up to a level of 40% blending with CR, which is then followed by an increase in interchain separation as the CR content is further increased. *Figure 7c* shows that the particle size remains unaltered up to a level of 40% blending with CR, followed by an asymptotic increase in size with further additions of CR to the blend.

These results indicate that PEMA consists of a large number of small crystallites, while CR contains a small number of large crystallites. This is confirmed by the broad and sharp crystalline melting temperatures of PEMA and CR, respectively (from d.s.c.).

Figure 7d shows that tan δ_{max} increases linearly with a decrease in the extent of crystallinity up to 10.5%, after which it increases asymptotically, thus leading to a concave curve[33].

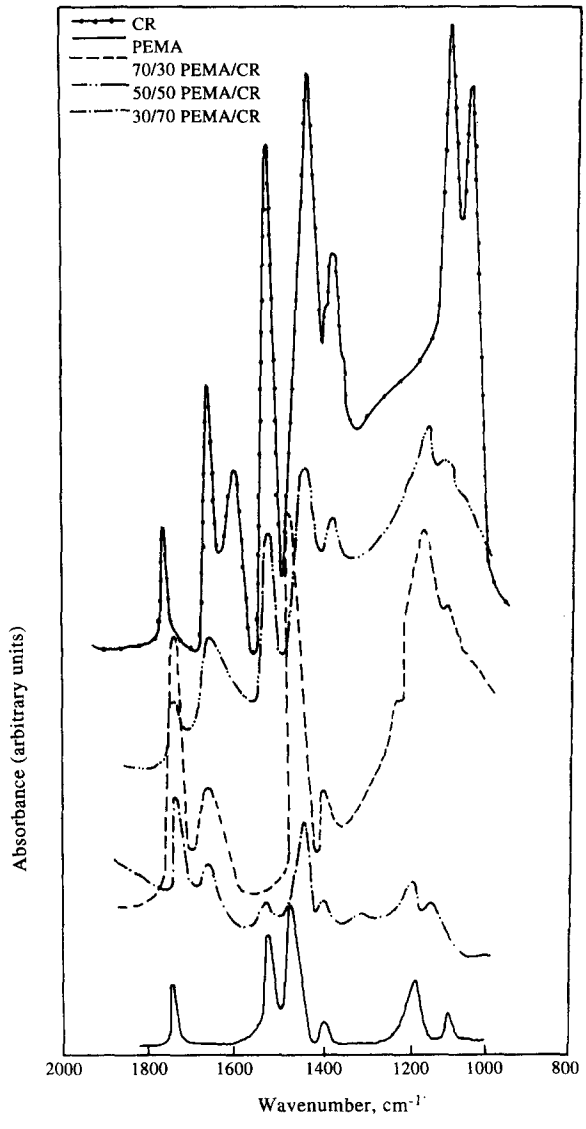

Figure 8 *FT* i.r. spectra of the various blends

FT*i.r. studies*

The *FT* i.r. absorption spectra of PEMA, CR, and the 70/30, 50/50 and 30/70 PEMA/CR blends are shown in *Figure 8*, with their characteristics group absorption bands being given in *Table 6*. The absorption band at 1309 cm^{-1} is due to the CH in-plane deformation of the C=C group of CR[21,34], while the bands at 1451 cm^{-1} are due to C–Cl overtone frequencies. The characteristic methyl (CH_3) asymmetric stretching band at 1465 cm^{-1}

observed for PEMA is shifted to 1455, 1448 and 1440 cm^{-1} by 30, 50 and 70% blending, respectively, with CR[35,36]. Identical amounts of shifting of this stretching frequency were observed for two different sets of polymer blends. This shift may be attributed to the dipolar interactions between the polar methyl acrylate and chloride groups of PEMA and CR. Due to this interaction, a slight positive (δ^+) centre is generated at the carbonyl carbon (as shown in *Scheme 1*), which weakens the O–C bond of the $-O-CH_3$ group, as evidenced from the lowering of the intensity of the methyl asymmetric stretching band of PEMA on blending with CR[35].

SEM studies

Cryogenically fractured surfaces of the individual polymers and their blends are shown in *Figure 9*. The scanning electron micrograph of PEMA shows deep cracks and the ridge patterns that are generated have no definite direction, whereas the micrograph of the elastomeric CR shows much smoother surfaces; these are full of hair-like cracks which resemble fibrils. This fibrilic nature is due to the brittle fracture of the CR. It is virtually impossible to keep the temperature of cryogenically cooled samples below −77°C during fracturing in the open atmosphere. All of the blends and pure PEMA have unconstrained T_gs in the region from −71 to

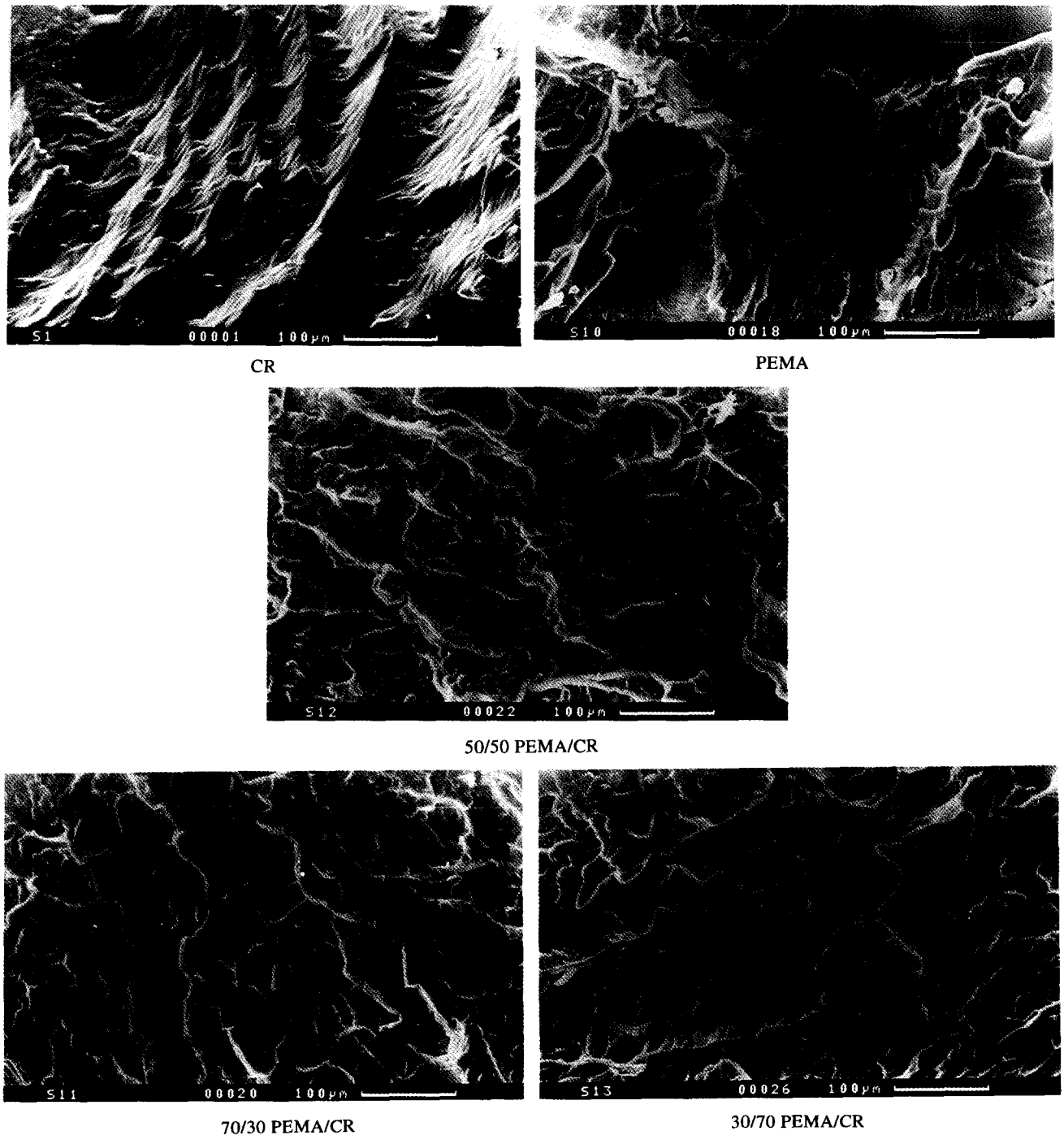

Figure 9 Scanning electron micrographs of cryogenically fractured surfaces of PEMA, CR, and their blends

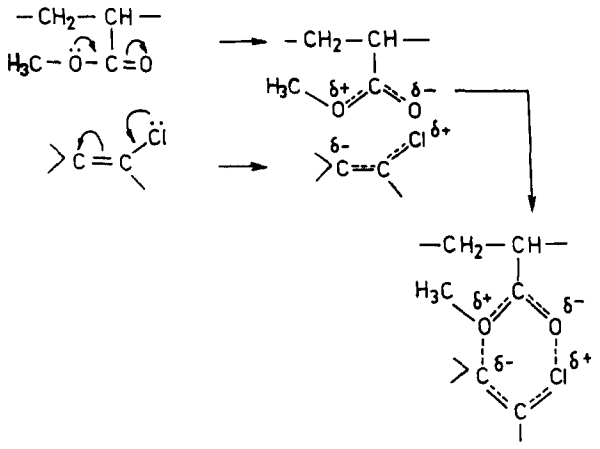

Scheme 1

$-77°C$, below which the resulting crystals take the fracture force. The characteristic fibrilic nature of pure CR is absent in all of the blends, while the ridges present in PEMA are well dispersed throughout the matrix for all blend compositions. We therefore conclude that CR and PEMA can be melt-blended homogeneously.

CONCLUSIONS

The results of our studies on the PEMA/CR blend system lead us to draw the following conclusions:

1. D.m.a. studies reveal that the crystal-constrained T_gs (main T_gs) of the blends follow the Fox equation.
2. D.s.c. studies also show that all of the blends exhibit a single T_g value. Increased contents of CR in the blends decrease the crystalline melting temperature of PEMA, as well as their negative interaction parameters.
3. From WAXD studies of the blends it is found that the extent of crystallinity of PEMA which contains small crystallites, decreases with increased contents of amorphous CR, where the latter has a large crystal particle size and a large interchain separation.
4. *FT*i.r. spectroscopic studies indicate that dipolar interactions occur between the PEMA and CR in the blends with different compositions, which is evidence for their miscibility.
5. Scanning electron micrographs of cryogenically fractured surfaces of the blends show homogeneity in mixing.

From the above, it can be concluded that PEMA and CR blends are miscible for all compositions.

REFERENCES

1 Paul, D. R. and Newman, S. 'Polymer Blends', Vol. 1, Academic, New York, 1978
2 Utracki, L. A. and Favis, B. D. in 'Handbook of Polymer Science and Technology' (Ed. N. P. Cheremisinoff), Vol. 4, Marcel Dekker, New York, 1989, p. 121
3 Akiyama, S., Komatsu, T. and Kaneko, R. *Polym. J.* 1975, **7**, 172
4 Coleman, M. M., Zarian, J., Varnell, D. F. and Painter, P. C. *J. Polym. Sci. Polym. Lett. Edn* 1977, **15**, 745
5 Kruse, W. A., Kirste, R. G., Hass, J., Schmitt, B. J. and Stein, D. J. *Makromol. Chem.* 1976, **177**, 1145
6 Utrachi, L. A. *Adv. Polym. Technol.* 1985, **5**, 33
7 Khambatta, F. B., Warner, F., Russel, T. and Stein, R. S. *J. Polym. Sci. Polym. Phys. Edn* 1976, **14**, 1391
8 Shultz, A. R. and Beach, B. M. *Macromolecules* 1974, **7**, 902
9 Sperling, L. H. *Polym. Eng. Sci.* 1984, **24**, 1
10 Feldman, D. and Rusu, M. *J. Polym. Sci. Polym. Symp. Edn.* 1973, **42**, 639
11 Boyd, R. H. *Macromolecules* 1984, **17**, 903
12 Hammer, C. F. *Macromolecules* 1971, **4**, 69
13 Casper, R. and Morbitzer, L. *Angew. Makromol. Chem.* 1977, **58/59**, 1
14 Amber, M. R. *J. Polym. Sci. Polym. Chem. Edn* 1973, **11**, 1505
15 Landi, V. R. *Appl. Polym. Symp.* 1974, **25**, 223
16 Elmqvist, C. and Svanson, S. E. *Eur. Polym. J.* 1976, **12**, 559
17 Kurian, J., Akhtar, S., Nando, G. B. and De, S. K. *J. Appl. Polym. Sci.* 1989, **37**, 1961
18 Fox, T. G. *Bull. Am. Phys. Soc.* 1956, **2**, 123
19 Nishi, T. and Wang, T. T. *Macromolecules* 1977, **10**, 421
20 Zhu, K. J., Chen, S. F., Ho, T., Pearce, E. M. and Kwei, T. K. *Macromolecules* 1990, **23**, 150
21 Socrates, G. 'Infrared Characteristic Group Frequencies', Wiley, New York, 1980
22 Moskala, E. J., Varnell, D. F. and Coleman, M. M. *Polymer* 1985, **26**, 228
23 Cesteros, L. C., Isasi, J. R. and Katime, I. *Macromolecules* 1993, **26**, 7256
24 Hermans, P. H. and Weidinger, A. *Makromol. Chem.* 1961, **24**, 44
25 Fava, R. A. (Ed.) 'Methods of Experimental Physics: Polymers', Vol. 16B, Academic, New York, 1973
26 Klug, H. P.. and Alexander, L. E. 'X-ray Diffraction Procedures for Polycrystalline and Amorphous Materials', Wiley, New York, 1954, p. 137
27 Lam, R. and Geil, P. H. *Polym. Bull.* 1978, **1**, 127
28 Boyd, R. H. *Polymer* 1985, **26**, 323
29 Lam, R. and Geil, P. H. *J. Macromol. Sci. Phys.* 1981, **20**, 37
30 Prest, W. M. and Porter, R. S. *J. Polym. Sci. Polym. Phys. Edn* 1972, **10**, 1639
31 Paul, D. R. and Atanirano, J. D. *Am. Chem. Soc. Div. Polym. Chem. Polym. Prep.* 1974, **15**, 409
32 Imken, R. L., Paul, D. R. and Barlow, J. W. *Polym. Eng. Sci.* 1976, **16**, 593
33 Boyd, R. H. and Aylwin, P. A. *Polymer* 1984, **25**, 340
34 Kole, S., De, P. P. and Tripathy, D. K. *Polymer* 993, **34**, 3732
35 Kemp, W. 'Organic Spectroscopy', 2nd Edn, ELBS, UK, 1987
36 Bovey, F. A., Bruch, M. D. and Kozlowski, S. A. *Macromolecules* 1985, **18**, 1418